Lawrence Berkeley National Laboratory

Title
Precipitation-Strengthened Austenitic Fe-Mn-Ti Alloys

Permalink
https://escholarship.org/uc/item/97b1z217

Authors
Chang, Keh-Minn
Morris, J W, Jr.

Publication Date
1977-06-01

PRECIPITATION-STRENGTHENED AUSTENITIC
FE-MN-TI ALLOYS

Keh-Minn Chang
and J. W. Morris, Jr.

June 1977

DISCLAIMER

PRECIPITATION-STRENGTHENED AUSTENITIC Fe-Mn-Ti ALLOYS

K. M. Chang and J. W. Morris, Jr.

Department of Materials Science and Mineral Engineering and
Materials and Molecular Research Division, Lawrence Berkeley Laboratory;
University of California, Berkeley, California 94720
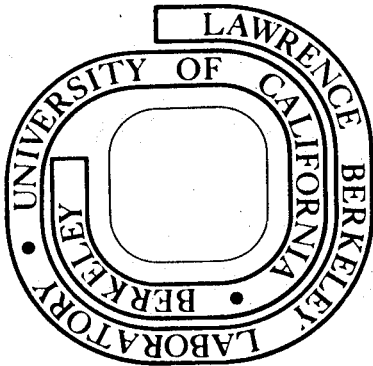
ABSTRACT

The precipitation of the intermetallic compounds in the Fe-20Mn-2Ti and Fe-28Mn-2Ti alloy systems has been investigated over the temperature range 700°C to 900°C by hardness measurements, optical and scanning electron microscopy, and X-ray diffraction. In both systems only the equilibrium Laves phase was observed. The precipitate was identified as a $C14(MgZn_2)$ type hexagonal Laves phase with a chemical composition close to $Fe_2(Ti,Mn)$. The precipitation in an as-annealed sample occurred predominantly in a heterogeneous manner, predominantly along grain boundaries.

The alloys were cold rolled between the solution annealing and aging processes. In addition to the high density of dislocations, martensitic phases were induced by deformation; a $\gamma \rightarrow \epsilon$ transformation occurred in the Fe-28Mn-2Ti alloy while a $\gamma \rightarrow \alpha'$ transformation was predominant in the Fe-20Mn-2Ti alloy. Subsequent aging was conducted at temperatures above A_f, which resulted in the matrices maintaining the austenitic form after cooling to room temperature. With sufficient nucleation sites, a large number of very fine precipitates formed randomly in the matrices within a short aging period. This work plus aging treatment resulted in an increase in yield strength. The enhancement of mechanical properties is due to the randomly distributed precipitates combined with the high defect density and fine substructure. Approximately 20% uniform elongation was observed in the tensile tests. This ductility is enhanced by the strain-induced transformation.

INTRODUCTION

Austenitic iron-base alloys containing high manganese content have been developed and commercially used for various purposes. The austenitic structure of these alloys is mechanically unstable unless a large amount of manganese or other austenite stabilizer is added.[1] The metastable parent phase undergoes a martensitic phase transformation when it is subjected to deformation at a temperature lower than M_d. To beneficially utilize this phenomenon, the thermomechanical treatments[2] have been applied to some high manganese steels.[3,4] The mechanically induced transformations, including both γ (fcc) $\rightarrow \varepsilon$ (hcp) and γ (fcc) $\rightarrow \alpha'$ (bcc) have been shown to improve the tensile strength and the ductility.

From an economic point of view, manganese is a very promising austenite stabilizing element for iron-base alloys. Substituting manganese for nickel in austenitic stainless steel, as in the AISI 200 Series, has been effectively utilized for more than twenty years in order to reduce materials cost without sacrificing properties.[5] Most commercial high manganese steels contain interstitial hardening elements, such as carbon or nitrogen,[6,7] which contribute to the strength of the matrix by forming precipitates of carbides or nitrides. The difficulty in processing and the thermal instability of interstitial precipitates put a limit on their desirability in high manganese steels. Therefore, efforts are underway to use intermetallic compounds to strengthen high manganese, iron-based alloys.

The occurrence of intermetallic phases in iron has been summarized by Nevitt.[8] Table I is a general resumé of possible phases based on B elements such as manganese, iron, cobalt and nickel with additions of A elements from the titanium, vanadium, chromium groups of the Periodic Table. Three factors: electron/atom ratio, atomic size, and compressibility, are important in

determining alloy chemistry. The phases listed in Table I can be classified into two groups on the basis of the atomic arrangement within their crystal structures. In one group there are the geometrically close packed phases which contain both octahedral and tetrahedral interstices e.g. B_3A. In the other group, there are the topologically close packed phases which contain only tetrahedral interstices, e.g. Laves (B_2A), σ, μ, and χ. Technically, B_3A is the most important intermetallic compound in austenitic iron alloys, due to its morphology with small interparticle distance, large volume percent, and preference for general precipitation. Further favorable factors are coherency with close lattice matching, and the high ductility of the phase compared with other precipitates.

Unfortunately, no such phase has been found with the B element being manganese or iron. The most likely phase to exist in Fe-Mn austenite is the B_2A Laves phase which as reported [9] embrittles alloys at room temperature but seems to have a strengthening effect at high temperatures. The embrittlement caused by Laves phases is attributed to the continuing precipitation along grain boundaries. By eliminating this continuous grain boundary precipitation, Laves phases can be effectively utilized to strengthen an iron matrix. Jin [10] was successful in spheroidization of the grain boundary Laves phase by cycling through the α-γ phase transformation. The fracture mode changed from inter-granular cleavage to ductile rupture.

The objective of the present study was to investigate the precipitation behavior in the Fe-Mn austenites containing titanium as the hardening element. Aging characteristics, precipitate distribution and identification, and mechanical property measurement were conducted on (1) completely austenitic and (2) ε-phase bearing austenitic Fe-Mn-Ti alloys. The Laves phases Fe_2Ti and Mn_2Ti have been observed in the binary phase diagrams. [11] The existence

of the compound Fe_2Mn in the Fe-Mn equilibrium diagram has been proposed by Soviet workers [12] though its existence is not commonly accepted. Determining the chemical composition of the precipitate which is thermodynamically favorable will help in further understanding the ternary phase diagram.

The Orowan [13] strengthening mechanism of second phase particles suggests that the strength of an alloy containing a dispersion of fine particles is determined by the spacing between particles. The precipitation of Laves phases cannot contribute much strengthening since, in most cases, these phases heterogeneously nucleate and grow continuously along grain boundaries. Intergranular fracture is likely to occur resulting in reduced ductility. If a large number of nucleation sites are introduced in the matrix before the aging process, however, rapid nucleation can take place and continuous grain boundary precipitation can be avoided. The kinetics of matrix precipitation is then much faster and separate fine precipitates with small spacings will form. This uniform matrix precipitation can be facilitated by the high density of dislocations generated by heavy deformation. [14] The stored strain energy of these defects will aid in the heterogeneous nucleation of Laves phases inside the matrix rather than along grain boundaries.

Following deformation the aging process can be conducted at a temperature just above A_f, so that the matrix phase will revert to the austenitic structure. With a highly deformed structure, isothermal aging requires less time and lower temperature since the precipitation kinetics is faster.

I. EXPERIMENTAL PROCEDURE

Alloys were prepared by induction melting under argon atmosphere using high purity (99.9%) iron, manganese, and titanium to produce cast ingots in 10 and 4.5 kg copper chill molds. The nominal and actual compositions of the alloys used in the present study are given in Table II. The ingots were homogenized at 1200°C for 24 hours under a partial pressure of argon gas (0.38 torr), forged to 26mm (for 10 kg ingots) and 13mm (for 4.5 kg ingots) thick plates, solution annealed at 1150°C for 1.5 hours under argon gas atmosphere, and water quenched. Some plates were cold rolled about 40% reduction in area to study the effects of cold work on the precipitation reaction. Tensile tests were conducted at room temperature in an Instron machine using flat tensile specimens of 25.4mm gauge length and 6.35mm x 3.175mm cross section at a cross-head speed of 2.0mm/min. Two specimens were tested for each data point. The 0.2% offset method was used to obtain the yield strength. The hardness of the specimens was measured as an average of five indentations with the elapsed time of 15 seconds. Quantitative measurements of the amounts and types of phases present were conducted using an X-ray diffractormeter utilizing transverse sections of the original plated materials to minimize the effects of preferred orientation, and the percentage of phases present were estimated by comparing the integrated diffraction intensities of the $(200)_\gamma$, $(10.1)_\varepsilon$, $(200)_\alpha$, peaks from a copper K_α source. The mathematical technique used is explained in detail by Cullity.[15] The identification of precipitate was performed by the X-ray diffraction method, and also energy dispersion analysis of X-ray (EDAX) on a scanning electron microscope. Optical metallographic specimens were chemically polished, and etched using a 5% nital solution. Schumann's reagent (100ml cold saturated $Na_2S_2O_3$ + 5gm $K_2S_2O_5$) was applied whenever the ε phase existed in a specimen since this reagent is reported [16] to be useful for delineating the ε phase. Thin foils for transmission electron microscopy were prepared by a jet electro-

polishing technique using a conventional chromic-acetic electrolyte. A
Hitachi HU-125 electron microscope operated at 100 kV was used for the
transmission microscopy.

II. RESULTS AND DISCUSSIONS

A. PHASE RELATIONS

The volume fractions of different phases observed by X-ray diffraction
analysis after various thermal and/or mechanical treatments are listed in
Table III. Fe-Mn alloys having more than 28 wt%Mn become fully austenitic (γ)
at room temperature. The hexagonal ε phase was not detected by the x-ray
technique in an as-annealed Fe-28Mn alloy, but traces of ε phase were observed
under the optical microscope (Fig. 1a). In the alloy with 20 wt%Mn, increasing
amounts of ε phase (up to about 70%) formed upon cooling from a solution
annealing to room temperature. A typical microstructure of mixed γ and ε phases
is shown in Fig. 1b. No body-centered cubic α' phase formed in either
alloy even when cooled to liquid nitrogen temperature (-196°C). These results
are consistent with previous observations.   Some authors [17,18] attribute
the formation of ε phase in the Fe-Mn system to the effect of Mn on (1) the
kinetics of austenite decomposition and (2) the stacking fault energy of the
austenite. With increasing Mn content, not only is the transformation
temperature lowered, but there is also a decrease in the austenitic stacking
fault energy. The combined effects of increasing Mn content is to accelerate
the $\gamma \rightarrow \varepsilon$ transformation as the austenite stacking fault energy approaches zero.

With the addition of titanium the amount of ε phase decreases dramatically
and more γ phase is retained at room temperature. The Fe-28Mn-2Ti alloy
was completely austenitic in the as-annealed condition (Fig. 1c). Less than
10% of ε phase formed in the Fe-20Mn-2Ti alloy (Fig. 1d). The influence
of Ti on the $\gamma \rightarrow \varepsilon$ transformation is not well understood. Previous workers [18]

observed that titanium additions can reduce the austenitic stacking fault
energy of some Fe-Ni-Cr alloys. Yeo [19] and Abraham, et al [20] found that
the M_s temperature of Fe-Ni-Ti alloys decreases with increasing Ti content.
Whether the stacking fault energy of the Fe-Mn austenite is lowered by
titanium additions is still unknown. However, it is clear from the present
results that Ti decreases the M_s temperature of the Fe-Mn austenite;
i.e. Ti is a strong austenite stabilizer for Fe-Mn alloys. This was further
shown by aging Fe-20Mn-2Ti alloys for long periods to precipitate Ti out
of the matrix. Isothermal overaging at 800°C for 20 days left about 1%
of the titanium in the matrix; the volume fraction of the ε phase increased
again to 44% (Table III).

B. KINETICS AND MORPHOLOGY OF
LAVES PHASE PRECIPITATION

1. Precipitation in the Fe-20Mn-2Ti Alloy:

The influence of temperature on the age hardening kinetics is shown
in Fig. 2. As expected, the lower the aging temperature, the longer the
time required to reach maximum hardness. The hardening response of the alloy
was very slow in the temperature range 700°C to 900°C; it took more
than 100 hours to achieve the maximum hardness plateau. No secondary
hardening was observed which suggests that only a single precipitation process
occurred.

On aging, precipitates nucleated first at grain boundaries and grew
continuously until a heavy network was formed. (Fig. 3a). Just before
a significant hardness increase, some precipitates were observed
within the grains. As the aging time increased, more and more precipitates
formed inside each grain, with an accompanying hardness increase as shown in
the age hardening curves. Precipitates inside grains appeared to line up along

planes parallel to γ-ε phase boundary. In later aging stages, the continuous precipitates along grain boundaries began to break up and individual particles were found to be spheroidized (Fig. 3b).

Apparently the precipitation process in the alloy is highly heterogeneous. Large surface energy is expected for the interface between the precipitate and the matrix. The alignment of precipitates inside grains along the former γ-ε interfaces is also in agreement with the above hypothesis. Though the γ-ε interfaces do not exist when the alloy is heated up to the aging temperature which is greater than A_f ($\sim$540°C), the distortion energy due to the martensitic transformation might still remain [21] to help the nucleation process. A high density of stacking faults inside grains introduced by the $\varepsilon \rightarrow \gamma$ transformation of the Fe-20Mn-2Ti alloy might also serve as the nucleation site for precipitation. The mechanism of spheroidization for the grain boundary precipitate at late aging stages needs further study; the precipitate growth and coarsening might play an important role in this phenomenon.

2. Precipitation in the Fe-28Mn-2Ti Alloy:

The hardening kinetics as a function of aging temperatures are shown in Fig. 4 for the Fe-28Mn-2Ti alloy; since the age hardening response is similar to that observed in the Fe-20Mn-2Ti alloy this indicates that the same kind of precipitation reaction took place. The aging response is more temperature dependent in this completely austenitic alloy. The hardness approaches its plateau within 100 hours at 900°C; but there was no obvious hardness increase in a sample aged at 700°C for more than 200 hours. Though the as-annealed hardness varied between the two alloys (R_B 72 for

Fe-20Mn-2Ti and R_B 62 for Fe-28Mn-2Ti), the total hardness increase at the plateau is almost the same. The hardness result can be explained by the morphology and distribution of precipitates. Fig. 5 shows a series of micrograph from samples aged at 800°C. In the early stage continuous precipitates rapidly developed along grain boundaries but contributed no hardness increase. The continuous precipitates can also be found along the incoherent interfaces of annealing twins but few precipitates occurred on coherent interfaces. This also supports the hypothesis that the precipitation occurs in a hetero-geneous manner which favors formation on high energy surfaces. Random nucleation started inside grains when most of the high energy surface utilized. The hardness gradually increased as the percentages of precipitates observed in grains increased. Spheroidization of grain boundary precipitates was also observed during the final stage of aging.

C. PRECIPITATE IDENTIFICATION

Samples of both alloys were aged at 800°C for 20 days to obtain precipitate sizes and volume fractions adequate for analysis. It is necessary to obtain precipitates with diameters greater than 2μ for EDAX analysis; and more than 5% in volume for X-ray diffraction.

Many extra diffraction peaks were detected in the X-ray diffraction patterns. Their corresponding interplanar spacings and relative intensities are listed in Table IV. These closely match the values in ASTM Powder Diffraction File for Fe_2Ti.[22] The crystal structure of the precipitate is the hexagonal Laves phase ($MgZn_2$ type, C14); each unit cell consists of 12 atoms as sketched in Fig. 6. The "a" parameter of the precipitate was determined from the (h k 0) reflections, using the extrapolation function of Nelson and Riley.[23] The "c" parameter was determined from the (00ℓ) reflection by the method of Taylor and Floyd[24] for hexagonal crystals. The values obtained are a=4.780Å, c=7.788Å, and c/a=1.629.

To obtain information about the chemical composition of the precipitates a SEM-EDAX study was made. Overetched specimens were examined in the scanning electron microscope, and some large precipitates ($\sim 5\mu$ diameter) were chosen for EDAX analysis. Fig. 7 presents comparative energy spectra showing that precipitates are rich in titanium and that they also contain manganese. The computer-analyzed data are given in Table V. The results are almost identical for the two alloys. The fraction of Fe in the precipitates is about 2/3. while that of the sum of Mn and Ti is about 1/3. Extraction replicas of specimens were also made in order to avoid the influence of the matrix phase during EDAX analysis. The results confirmed the above observations. The identity of the precipitates thus appears to be $Fe_2(Ti, Mn)$ in both alloys. The crystal structure of precipitates is like that of Fe_2Ti, with Mn atoms sitting at some Ti lattice sites. There also exists the possibility that a small fraction of Mn atoms replace Fe atoms in the precipitates. This may be the measured Fe concentration is somewhat less than the ideal stoichiometric ratio 2/3.

D. EFFECTS OF COLD WORK ON PRECIPITATION

It is not surprising that direct precipitation of Laves phases does not strengthen the solution-treated Fe-Mn-Ti austenites significantly. The inter-particle spacing between the aged precipitates formed inside grains is too large to be an effective obstacle to dislocation motion. The reason for this ineffective precipitation is that the alloys do not have enough beneficial nucleation sites for precipitation of Laves phase. The nucleation sites are not uniformly distributed throuhgout the grains. In order to overcome this problem, about 40% reduction by cold rolling was conducted on both alloys between the solution annealing and the aging processes.

The mechanical instability of high Mn austenites has been investigated by many previous workers.[1,3,4] These alloys undergo a partial martensitic phase transformation under heavy deformation at room temperature. In addition to the increase of defect and dislocation density, cold work induces elastic and plastic strain energy which raises the transformation temperature to the ambient temperature. The volume fraction of induced phases in the cold-worked samples is shown in Table III. A large amount of the α' phase and some ε phase appeared in the Fe-20Mn-2Ti alloy after cold rolling. Electron microscopy revealed that the induced α' phase is dislocated martensite with a high density of dislocations inside the martensite lathes (Fig. 8). Thin sheets of induced ε phase were also observed on edge parallel to one another. On the other hand, there is some ε phase formed in the Fe-28Mn-2Ti alloy after cold working, but no α' phase was observed. These induced ε sheets look wavy and bent somehow, though they are parallel to one another in series. More detailed examination by electron microscopy verified the above observation (Fig. 9). High dislocation densities were observed in the untransformed matrix.

Like the usual martensite obtained by thermal treatment, the induced phase, ε or α', in the cold worked alloys was reverted to austenite when the sample was reheated to high temperature. The dilatometry results indicated that A_f' is approximately 540°C. The subsequent quenching gave almost the same phase relation as that of a sample quenched from the solution annealing temperature. The Fe-20Mn-2Ti alloy was reheated to 800°C after cold-rolling, and then aged at that temperature. The kinetics of precipitation is accelerated by pre-deformation; very fine precipitiates of Laves phase covered the entire structure in one hour aging (Fig. 10a). The precipitates were randomly distributed throughout the whole specimen, no continuous

grain boundary precipitate was found. The very low diffusivity of the substitutional elements, Mn or Ti, in the austenite matrix makes precipitate growth or coarsening very difficult. No evidence of overaging was observed even after aging for 96 hours (Fig. 10b). After fully recovering from cold working, the alloy maintained a high level of hardness ($R_c \approx 26$) which was no doubt attributed to the fine, randomly distributed precipitates.

Closer examination of the precipitates formed in the cold worked plus aged alloys was carried out using the electron microscope. It is very difficult to index the area diffraction (SAD) patterns and to find out the orientation relationship of the precipitates with respect to the matrix. Heavy deformation of the alloys before aging will distort the matrix causing precipitate misorientation with respect to one another even though the Laves phase has a characterisitic orientation with the austenite. In the Fe-28Mn-2Ti alloy, the precipitates lined up along a specific orientation, which was believed to be the stacking fault plane. The precipitate size was less than 0.3μ in diameter. A high density of dislocations still remained in the matrix after aging for one hour at 700°C (Fig. 11a). The precipitates formed in the Fe-20Mn-2Ti alloy was denser and more random in distribution. Lath boundaries of previous α' martensites were decorated by the precipitate in some instances, but no continuous networks were observed (Fig. 11b).

E. MECHANICAL PROPERTIES

Both as-annealed alloys exhibited a low yield strength (~30ksi) and high elongation (~75%). X-ray diffraction of the broken tensile specimens showed phase contents similar to those obtained after cold rolling; the mechanically induced transformation also occurs during tensile testing. In both stress-strain curves the ultimate point, where the tensile specimen

started to neck, was delayed to a large elongation with very low strain hardening rate. The final fracture of the specimen occurred rapidly after passing the ultimate point. This is a typical feature of alloys with a mechanically induced transformation. The ultimate strength increases with increasing amounts of deformation-induced second phase. The stress increment of about 20ksi higher tensile strength for the Fe-20Mn-2Ti alloy is apparently due to the fact that the α' martensite is much stronger than the ϵ-phase.

Specimens aged after annealing reached full hardness after 100 hours at 800°C. Their grains are relatively large, (200 ~ 500µ), surrounded by a nearly continuous network of Laves phase. A large grain size and heavily decorated grain boundaries are both detrimental to the ductility. The intergranular fracture mode was observed in broken tensile specimens of both alloys as shown in Fig. 12. No significant strengthening effect occurred due to the large interparticle spacing between the precipitates inside the grains. The yield strength increased by ~5 ksi for the Fe-28Mn-2Ti alloy and ~10 ksi for the Fe-20Mn-2Ti alloy.

The stress-strain curves of the alloys which were cold worked and/or aged at 700°C for 1 hour are shown in Fig. 13. The yield strength was observed to increase to 107 ksi for the Fe-20Mn-2Ti alloy and to 90 ksi for the Fe-28Mn-2Ti alloy by use of a cold-working plus aging treatment. The difference in yield strength in the two different alloys may come from the existence of ϵ phase and the difference in the cold work plus aging process. Unlike the cold worked alloys which reached the ultimate point without much plastic deformation, the cold work plus aging alloys exhibited retarded necking with very large uniform elongation. This is believed to be the result of mechanically induced transformation.

The yield strength, tensile strength, and elongation of alloys with the cold work plus aging process are shown in Fig. 14 a function of aging temperature. For one hour aging times, both alloys revealed a monotonically decreasing yield strength for increasing aging temperature. The elongation showed a peak in the temperature range 650°C to 800°C. A similar result was observed in the thermal cycling processing of the TRIP steel.[25] No obvious change in elongation was observed for aging times up to 4 hours, although the yield strength kept decreasing with aging time. The fracture surface of the broken tensile specimen was unusual, in that it was neither the dimpled rupture of ductile failure like the as-annealed or the cold worked samples nor the intergranular cleavage of brittle fracture like the simple aged specimens. For the Fe-20Mn-2Ti alloy, in which $\gamma \rightarrow \alpha'$ martensite transformation is predominant, fracture surface perpendicular to the tensile axis was formed. Very tiny cups and cones spread over the whole fracture surface (Fig. 15a). On the other hand, the Fe-28Mn-2Ti alloy, in which only the $\gamma \rightarrow \epsilon$ transformation occurred, exhibited a fracture surface consisting of several tilted planes. In addition to the dimple rupture, a lamellar pattern was observed (Fig. 15B). The exact mechanism responsible for these fracture surfaces has not been established.

III. CONCLUSIONS

1. Precipitation in the Fe-20Mn-2Ti and Fe-28Mn-2Ti systems proceeds by the formation of single particles of equilibrium Laves phase, $Fe_2(Mn,Ti)$, hexagonal C14 type ($MgZn_2$). No transition phase was detected.

2. Precipitation in the as-annealed structure occurs by heterogeneous nucleation; heavy networks of Laves phases form first along the grain boundary before individual precipitates appear inside grains. No significant age - hardening is observed but intergranular fracture takes place due to the Laves phase precipitates.

3. Cold rolling after solution annealing provides numerous efficient nucleation sites beneficial to subsequent aging. The precipitate nucleation mode changes from grain boundary to separate heterogeneous sites inside grains. A desirable microstructure, in which fine precipitates are randomly distributed, is then obtained.

4. Enhancement of the mechanical properties of Fe-Mn austenites can be achieved through the combination of cold work, fine precipitates, and mechanically induced transformation.

5. Titanium additions can stabilize the austenite in Fe-Mn alloys.

ACKNOWLEDGEMENTS

REFERENCES

1. C. H. White and R. W. K. Honeycombe: J. Iron Steel Inst., 1962, Vol. 200, p. 457.

2. V. F. Zackay, E. R. Parker, D. Fahr, and R. Bush: Trans. ASM, 1967, Vol. 60, p. 252.

3. D. J. Drobjak and J. Gordon Parr: Met. Trans., 1970, Vol. 1, p. 1521.

4. K. Sipos, L. Remy, and A. Pineau: Met. Trans.A, 1976, Vol. 7A, p. 857.

5. R. Franks, W. Binder, and J. Thompson: Trans. ASM, 1955, Vol. 47, p. 231.

6. J. A. Douthett: Metal Progr., 1975, Vol. 108, No. 3, p. 50.

7. Metal Progr., 1976, Vol. 110, No. 5, p. 72.

8. M. V. Nevitt: Electronic Structure and Alloy Chemistry of the Transition Elements, p. 101, Interscience Publishers, New York, 1963.

9. K. Bungardt and G. Lennartz: Arch. Eisenh., 1962, Vol. 33, p. 251.

10. S. Jin: M.S. Thesis, U. of Calif., Berkeley, California, (1971).

11. M. Hansen: Constitution of Binary Alloys, McGraw-Hill, New York, 1958.

12. E. M. Sokolovskaya, A. T. Grigorév, and Yu. F. Altunin: Russ. J. Inorg. Chem., 1962, Vol. 7, p. 1464.

13. E. Orowan: Symposium on Internal Stress, Inst. of Metals, London, 1947, p. 451.

14. J. E. Bailey: Phil. Mag., 1960, Vol. 5, p. 833.

15. B. D. Cullity: Elements of X-Ray Diffraction, p. 388, Addison-Wesley, California, 1956.

16. H. Schumann: Arch. Eisenh., 1967, Vol. 38, p. 647.

17. A. Holden, J. D. Bolton, and E. R. Petty: J. Iron Steel Inst., 1971, Vol. 209, p. 721.

18. S. Barnartt, R. Stickler, and D. van Rooyen: Corrosion Sci., 1963, Vol. 3, p. 9.

19. R. B. G. Yeo: Trans. TMS-AIME, 1963, Vol. 227, p. 884.

20. J. K. Abraham and J. S. Pascover: Trans. TMS-AIME, 1969, Vol. 245, p. 759.

21. G. Krauss, Jr. and M. Cohen: Trans. TMS-AIME, 1962, Vol. 224, p. 1212.

22. G. R. Speich: Trans. TMS-AIME, 1962, Vol. 224, p. 850.

23. J. B. Nelson and D. P. Riley: Proc. Phys. Soc. (London), 1945, Vol. 57, p. 60.

24. A. Taylor and R. W. Floyd: Acta Cryst., 1950, Vol. 3, p. 285.

25. T. J. Koppeneal, Met. Trans., 1972, Vol. 3, p. 1549.

Table I.   OCCURRENCE OF PHASES IN BINARY AND TERNARY TRANSITION ELEMENT SYSTEMS

| | | Group IV (4e/a) | | | Group V (5e/a) | | | Group VI (6e/a) | | BB' |
B Transition Element	Ti	Zr	Hf	V	Nb	Ta	Cr	Mo	W	
Mn (7e/a)	B_2A	B_2A	B_2A		B_2A	B_2A				
				BA						
	X	X	X	X	X	X	X	X	X	
	σ			σ			σ	σ		
Fe (8e/a)	B_2A	B_2A	B_2A		B_2A	B_2A		B_2A	B_2A	
				BA						FeAl
	X			X				X		FeCo
				σ	σ	σ	σ	σ		
Co (9e/a)	B_2A	B_2A	B_2A	B_3A	B_2A	B_2A		B_3A	B_3A	
	BA	BA	BA							CoAl
				X				μ	μ	
	G	G	G	σ	G	G	σ	σ		
Ni (10e/a)	B_3A			B_3A	B_3A			B_3A		
	BA			X						β
				σ	μ	μ	σ			(NiAl)
	G	G	G	G	G	G				

* μ: B_7A_6; G: $A_6B_{16}Si_7$; σ: $B_4A \sim BA_4$; χ: $B_4A \sim BA$

18

Table II. CHEMICAL COMPOSITION OF ALLOYS

Ingot No.	Weight	Designation	Composition wt%		
			Fe	Mn	Ti
755-1	10 kg	Fe-20Mn	Bal.	19.11	--
755-2	10 kg	Fe-20Mn-2Ti	Bal.	18.66	1.70
7511-4	4.5 kg	Fe-28Mn-2Ti	Bal.	27.29	1.59
7511-10	4.5 kg	Fe-28Mn	Bal.	27.34	--
766-17	10 kg	Fe-20Mn-2Ti	Bal.	19.07	1.74
766-18	10 kg	Fe-28Mn-2Ti	Bal.	27.93	1.69

The impurity levels: C = 0.004%; N = 0.002%;

O = 0.002%; P = 0.004%; Si < 0.01%; S = 0.006%.

Table III.   DETERMINATION OF VOLUME PERCENTAGE OF PHASE
             PRESENT BY X-RAY ANALYSIS

Designation	Treatment	Phase volume percentage		
		γ	ϵ	α'
Fe-20Mn	AN	30.0	70.0	--
Fe-20Mn-2Ti	AN	90.4	9.6	--
Fe-20Mn-2Ti	AN+800°C/20 days	56.0	44.0	--
Fe-20MN-2TI	AN+CW	51.0	20.0	29.0
Fe-20Mn-2Ti	AN+CW+800°C/96 hrs	91.2	8.8	--
Fe-28Mn	AN	100.0	--	--
Fe-28Mn-2Ti	AN	100.0	--	--
Fe-28Mn-2Ti	AN+800°C/20 days	100.0	--	--
Fe-28Mn-2Ti	AN+CW	93.6	6.4	--
Fe-28Mn-2Ti	AN+CW+700°C/1 hr	100.0	--	--

AN: Annealed at 1100°C for 1.5 hrs.

CW: 40% reduction of cold rolling.

Table IV.   INTERPLANAR SPACING OF THE PRECIPITATES

Precipitates				Standard values for Fe_2Ti	
2θ*	d	I/I_1	(hkl)	d	I/I_1
--	--	--	100	4.133	10
--	--	--	002	3.889	10
--	--	--	101	3.649	10
37.6	2.390	30	110	2.388	30
41.0	2.199	90	103	2.199	100
--	--	--	200	2.068	10
44.4	2.039	90	112	2.038	100
45.3	2.001	100	201	1.998	100
46.6	1.947	40	004	1.947	30
49.85	1.828	20	202	1.828	30
51.8	1.763	10	104	1.760	10
--	--	--	203	1.620	10
--	--	--	300	1.382	10
70.2	1.339	40	123	1.341	60
72.65	1.330	40	006	1.302	60
76.4	1.246	30	205	1.247	60
--	--	--	124	1.223	10
80.25	1.195	40	220	1.196	60

*$CuK\alpha$ radiation with $\lambda = 1.54$Å

Table V.   DETERMINATION OF CHEMICAL COMPOSITION
           OF THE PRECIPITATES BY EDAX

Designation		Concentration (wt%)		
		Fe	Mn	Ti
Fe-20Mn-2Ti	matrix	78.90	19.44	1.66
	precipitate	63.60	14.80	21.60
Fe-28Mn-2Ti	matrix	69.76	29.34	0.90
	precipitate	62.90	14.30	22.80

*Specimens were aged at 800°C for 20 days.

FIGURE CAPTIONS

1. Optical micrographs of as-annealed Fe-Mn(-Ti) alloys: (a) Fe-28Mn; (b) Fe-20Mn; (c) Fe-28Mn-2Ti; (d) Fe-20Mn-2Ti.

2. Age-hardening curves of the Fe-20Mn-2Ti alloy.

3. Precipitation of the Fe-20Mn-2Ti alloy aged at 800°C for: (a) 2 hrs; (b) 48 hrs.

4. Age-hardening curves of the Fe-28Mn-2Ti alloy.

5. Precipitation of the Fe-28Mn-2Ti alloy aged at 800°C for: (a) 4 hrs; (b) 16 hrs; (c) 48 hrs.

6. Atomic arrangement in the unit cell of the $C14(MgZn_2)$ crystal.

7. EDAX for the precipitation of the Fe-20Mn-2Ti alloy.

8. Transmission electron micrograph of the cold-rolled Fe-20Mn-2Ti alloy.

9. Transmission electron micrograph of the cold-rolled Fe-28Mn-2Ti alloy: (a) bright field; (b) dark field.

10. Microstructures of the worked plus aged Fe-20Mn-2Ti alloy: (a) CW+700°C 1hr; (b) CW+700°C 96hrs.

11. Transmission electron micrographs of worked plus aged specimens: (a) Fe-28Mn-2Ti; (b) Fe-20Mn-2Ti.

12. Tensile fracture surfaces of simple aged specimens: (a) Fe-20Mn-2Ti; (b) Fe-28Mn-2Ti.

13. Engineering strain-stress curves of cold-worked and worked plus aged specimens.

14. The effect of aging temperature (for 1hr) on strength and elongation of cold-worked specimens.

15. Tensile fracture surfaces of worked plus aged specimens: (a) Fe-20Mn-2Ti; (b) Fe-28Mn-2Ti.

a

b
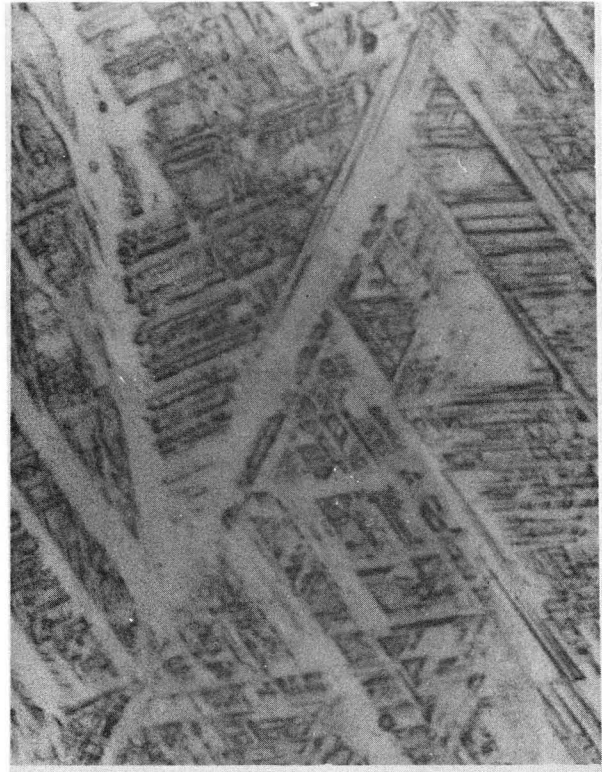
10μm
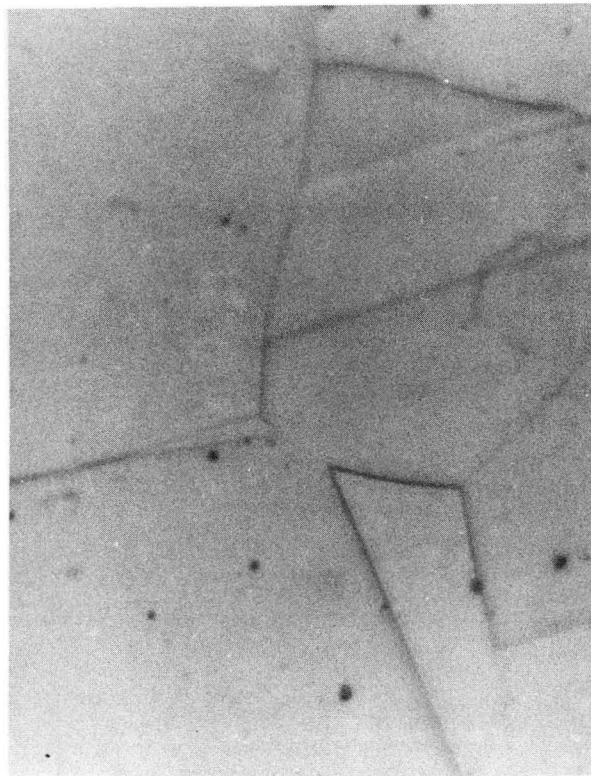
c
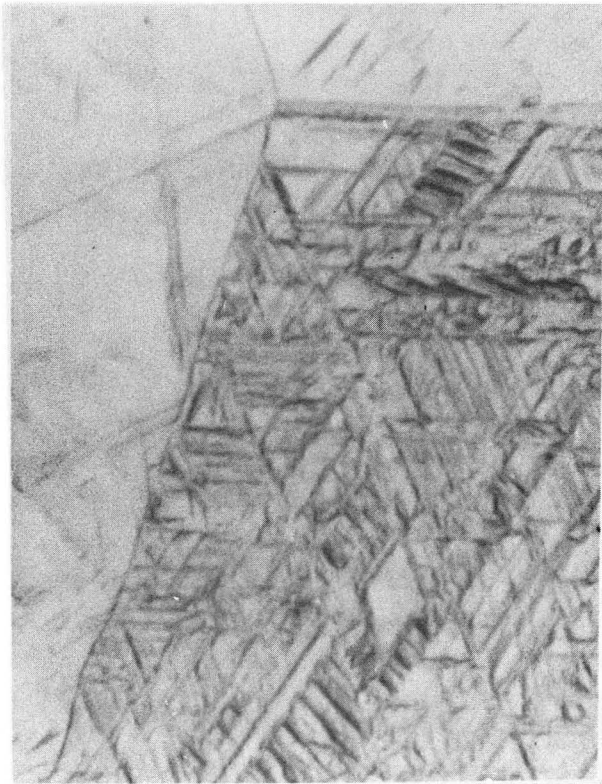
d

XBB 778-7376

Fig. 1
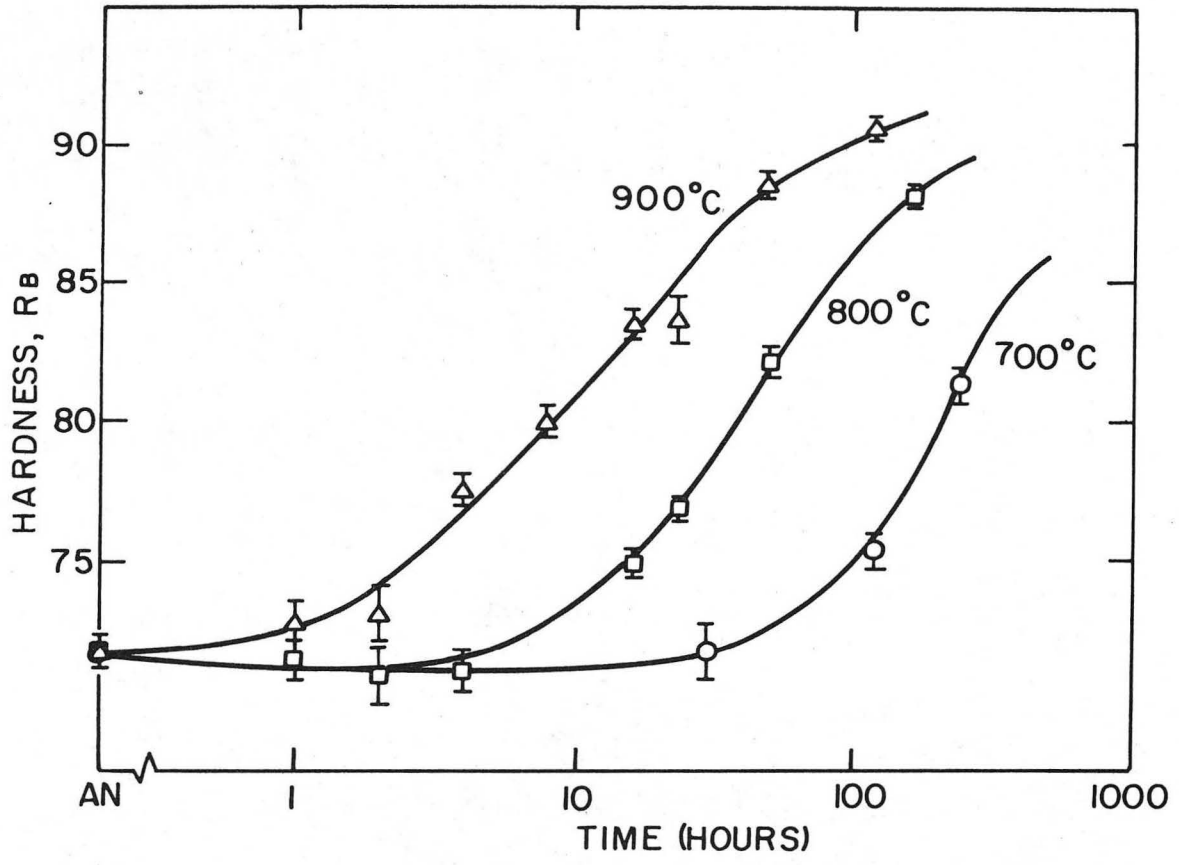
XBL 7610-7652

Fig. 2

a

0 μm
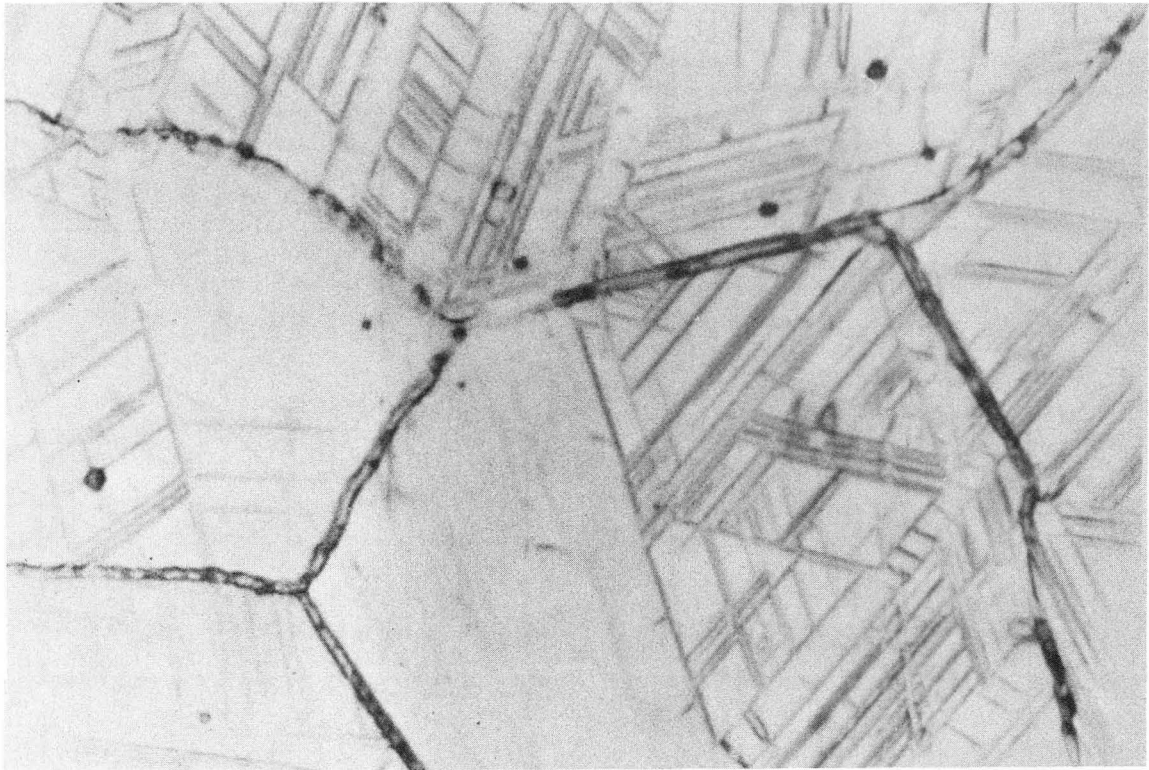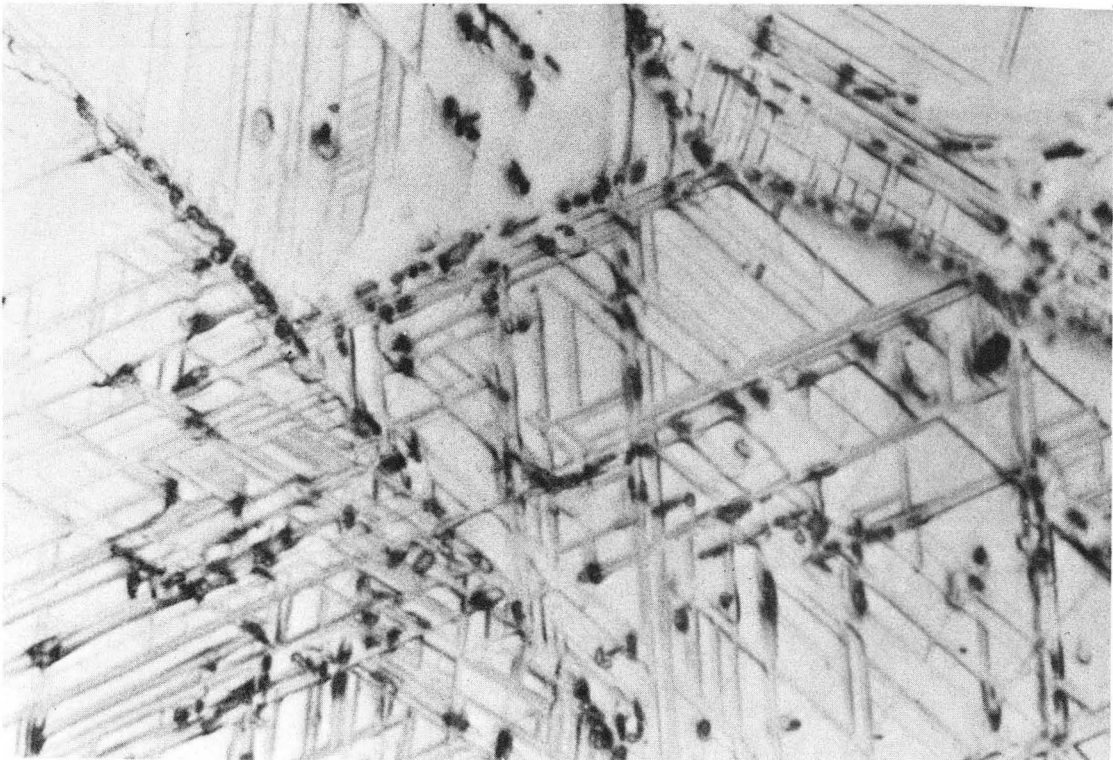
b   XBB 769 8584

Fig. 3
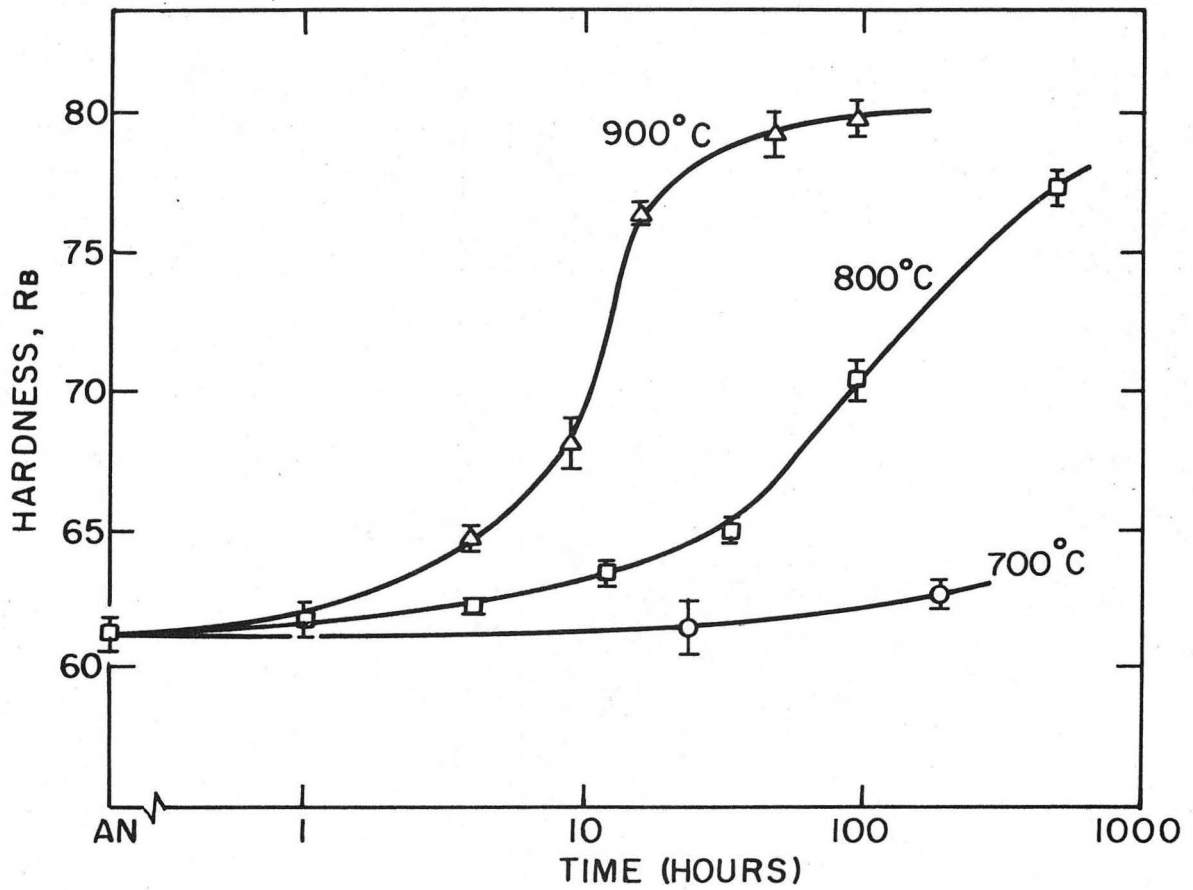
Fig. 4
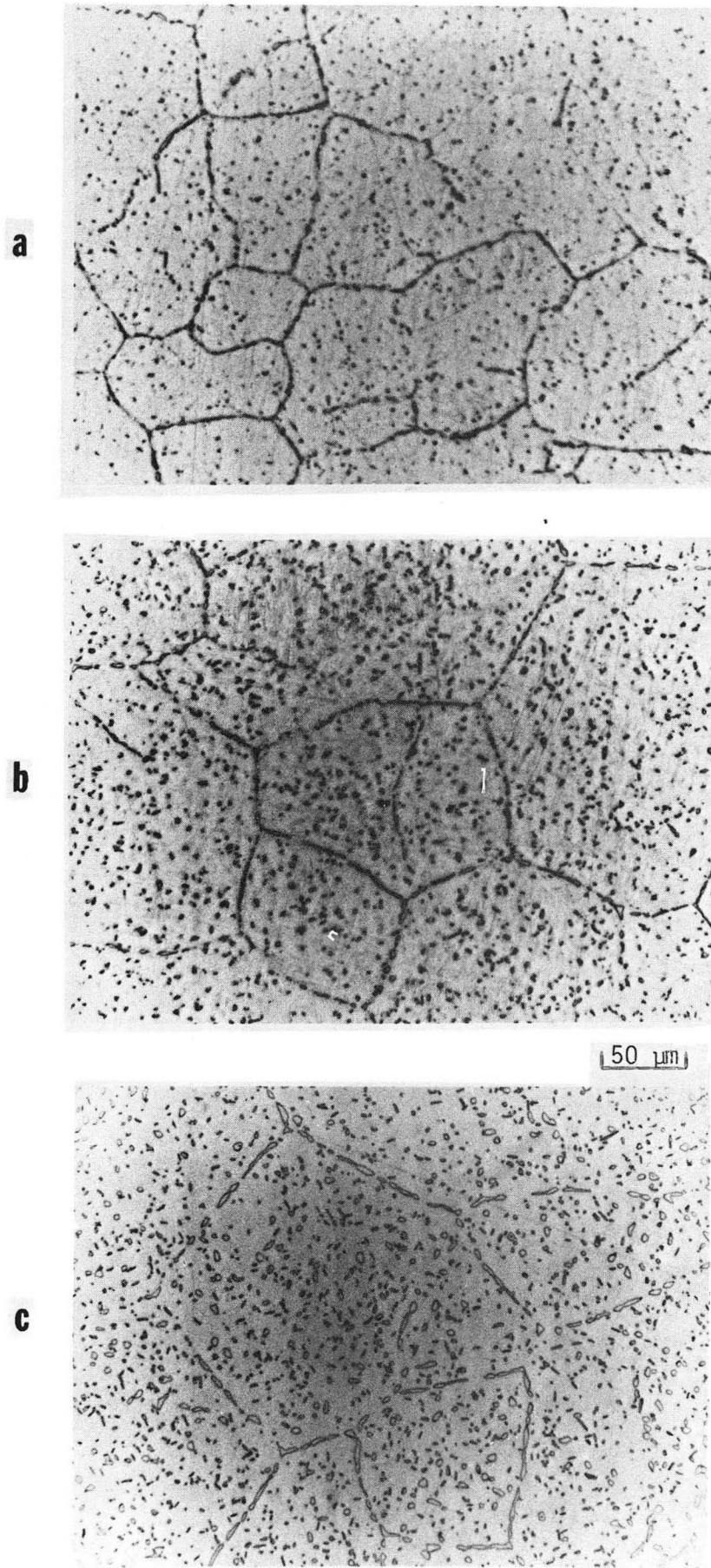
Fig. 5

C 14 (Mg Zn$_2$ type)   Hexagonal D$_{6h}^4$ − P 6$_3$/mmc

4Mg (C$_{3v}$): $\pm (\frac{1}{3}, \frac{2}{3}, z), \pm (\frac{1}{3}, \frac{2}{3}, \frac{1}{2} - z)$; $z = \frac{1}{16}$

2Zn (D$_{3d}$): (OOO), (OO$\frac{1}{2}$)

6Zn (C$_{2v}$): $\pm (X, 2X, \frac{1}{4}), \pm (\overline{2X}, \overline{X}, \frac{1}{4})$; $X = \frac{1}{6}$
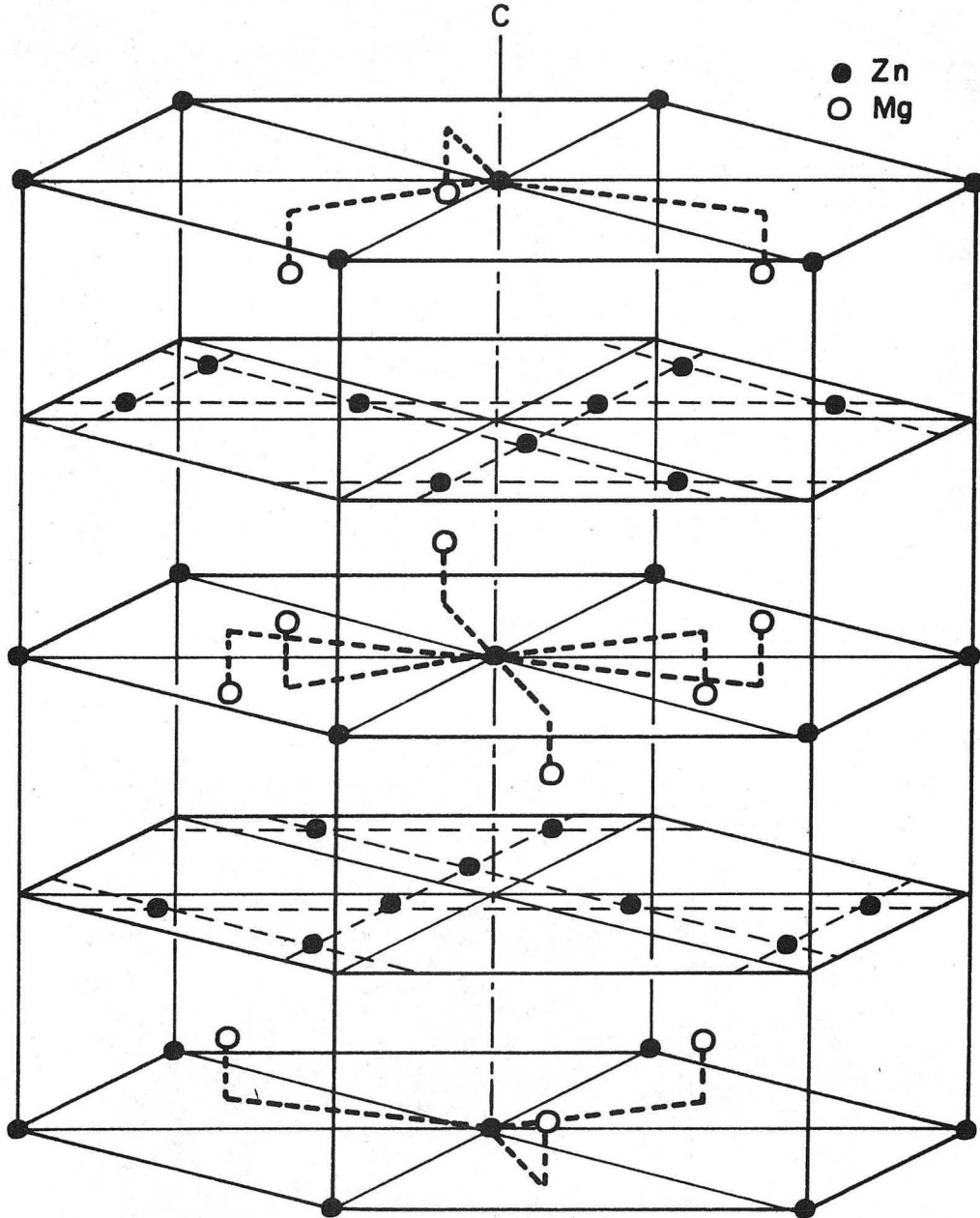
XBL 7611-7810

Fig. 6

5 μm

XBB 769-8583

Fig. 7

1 μm

XBB 773-1950

Fig. 8

BF (a) 0.5 μm

DF (b) XBB 773-1948

Fig. 8

a
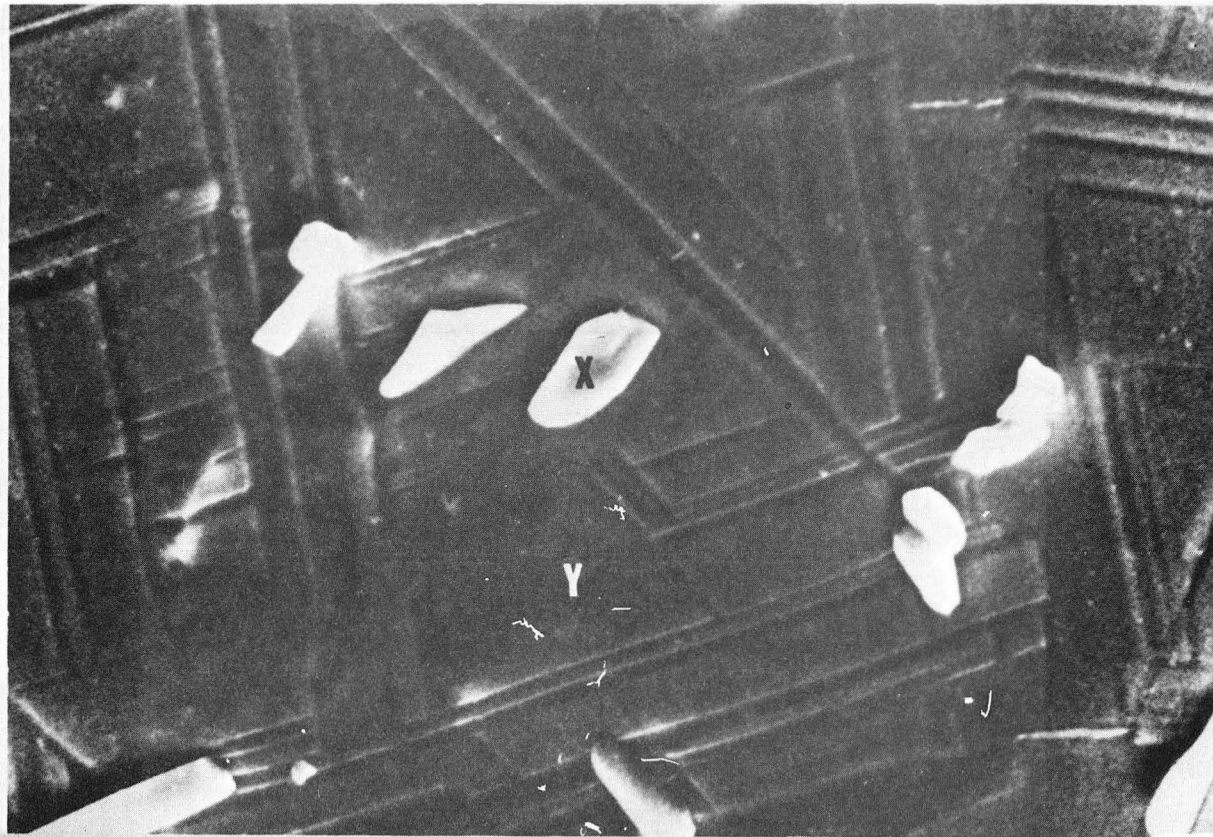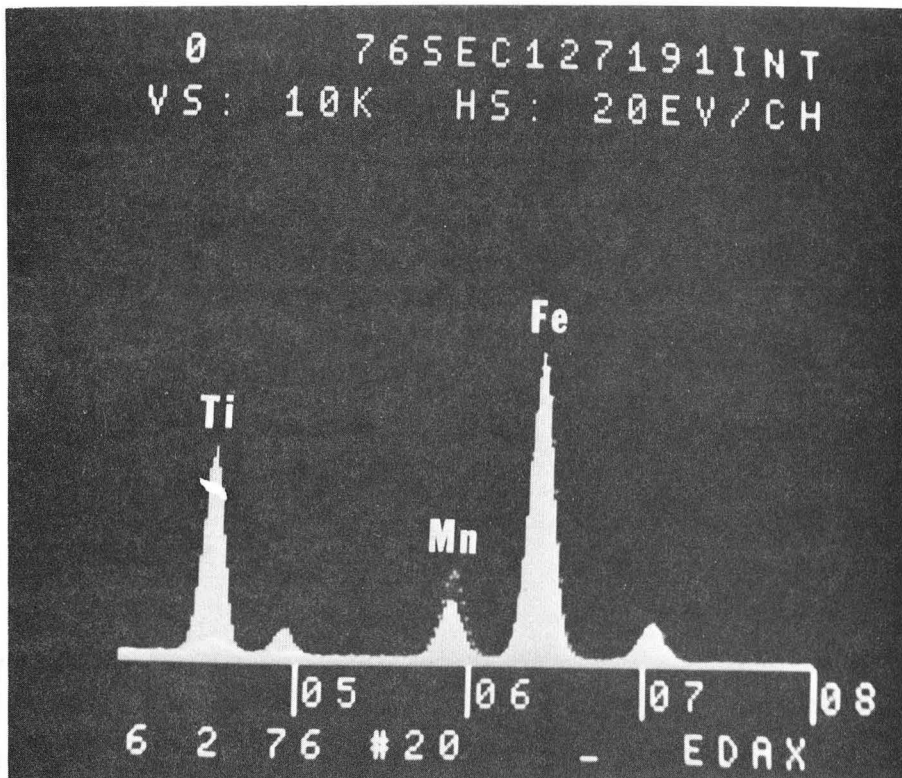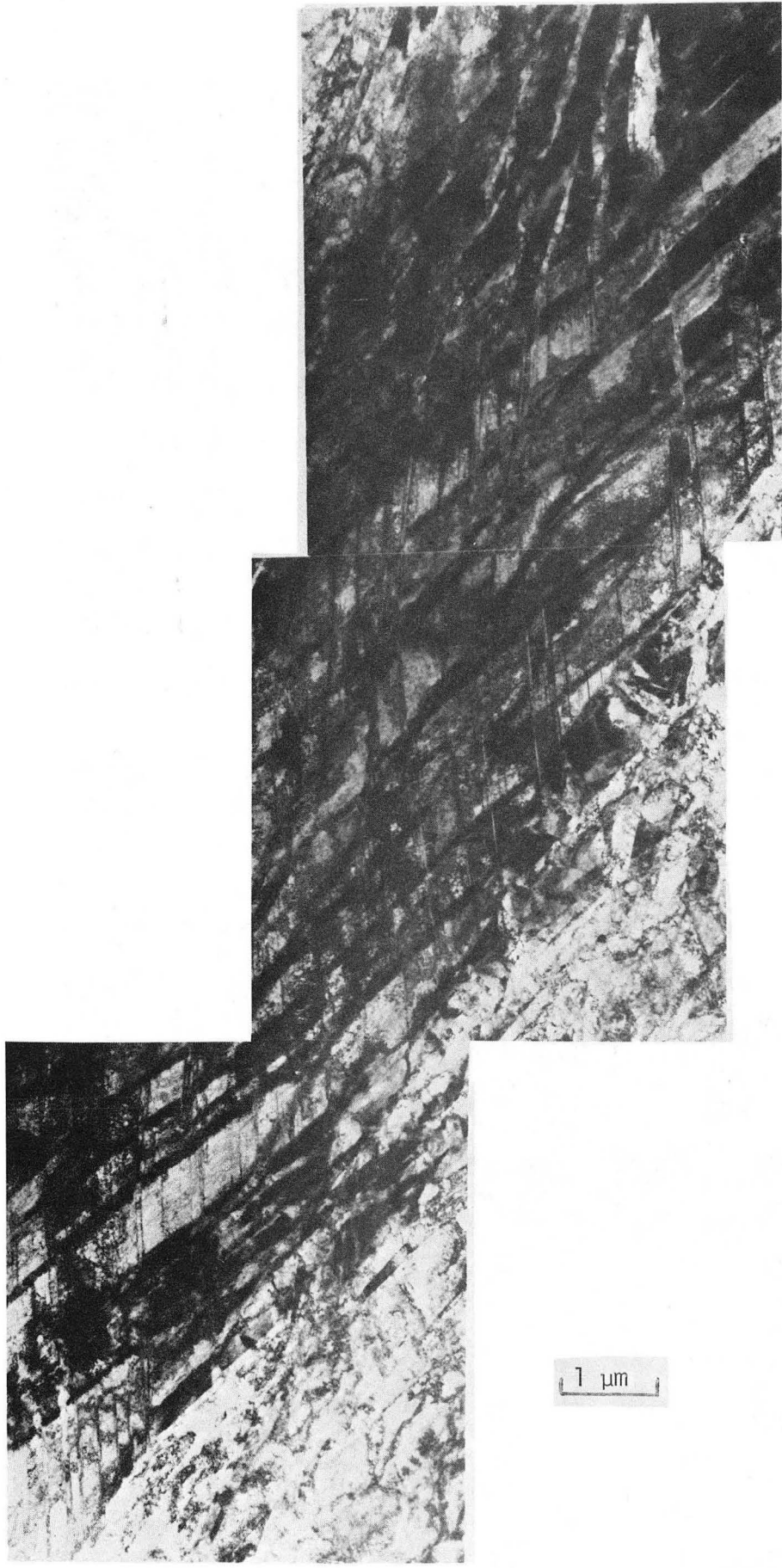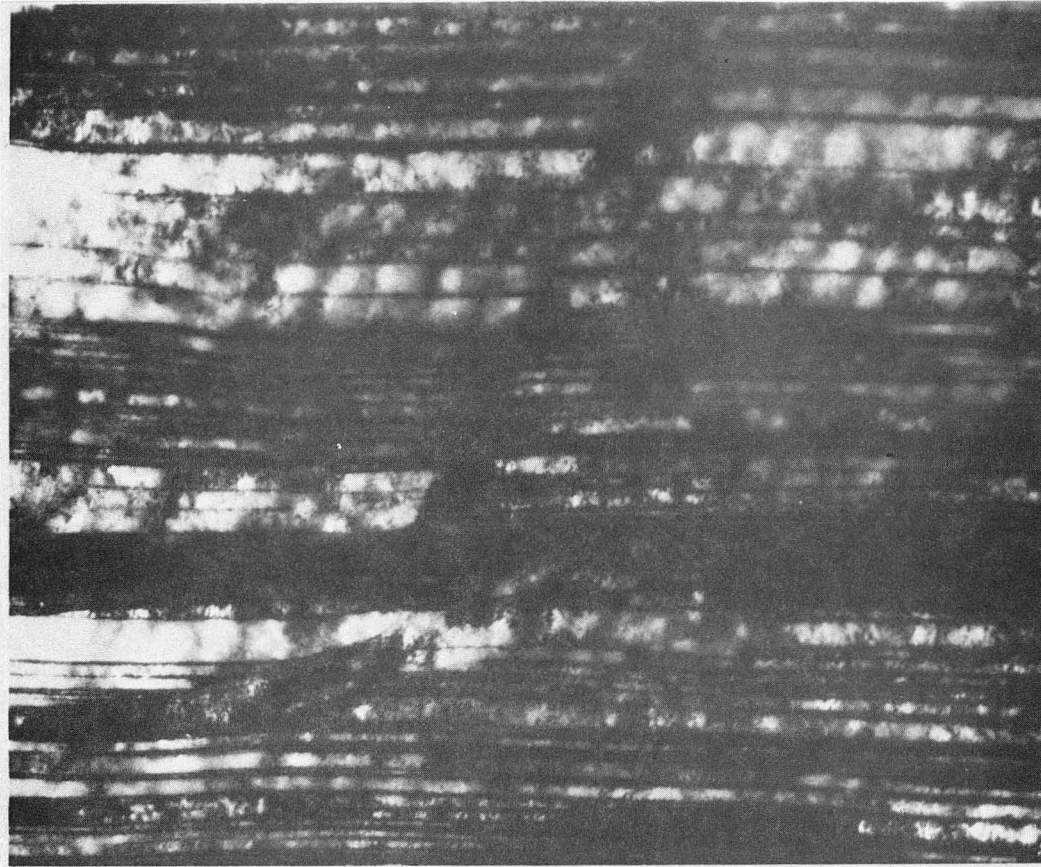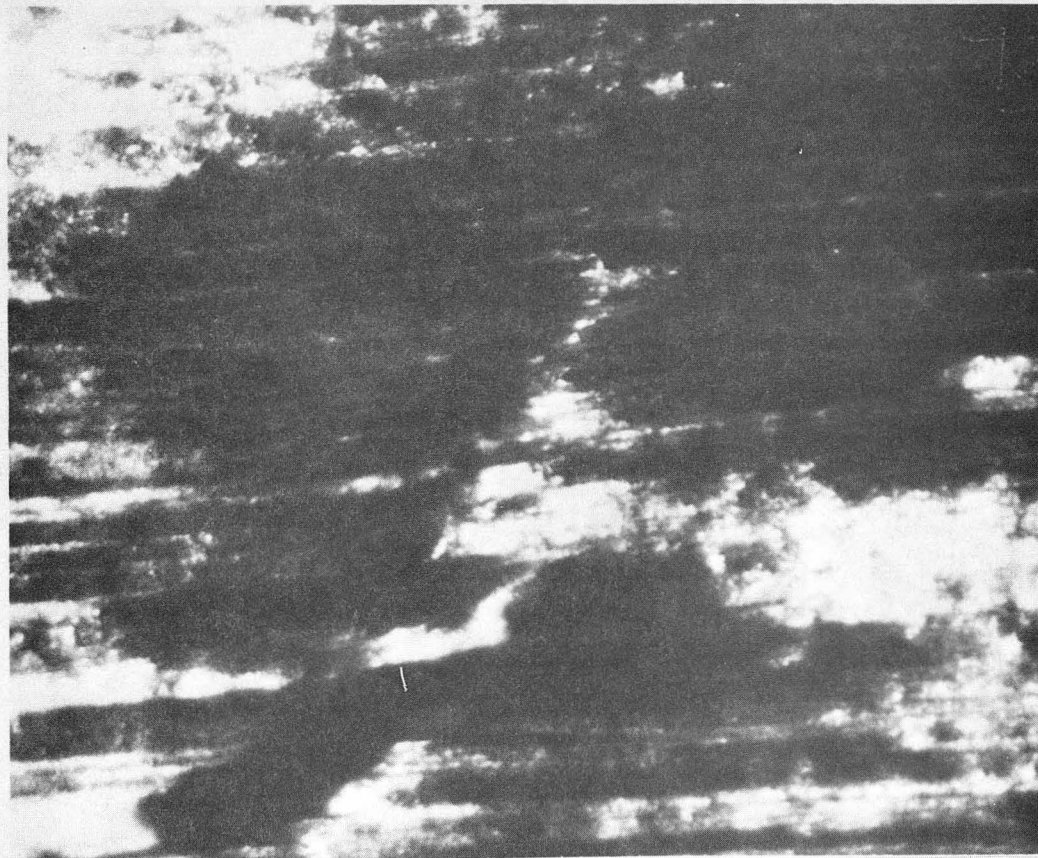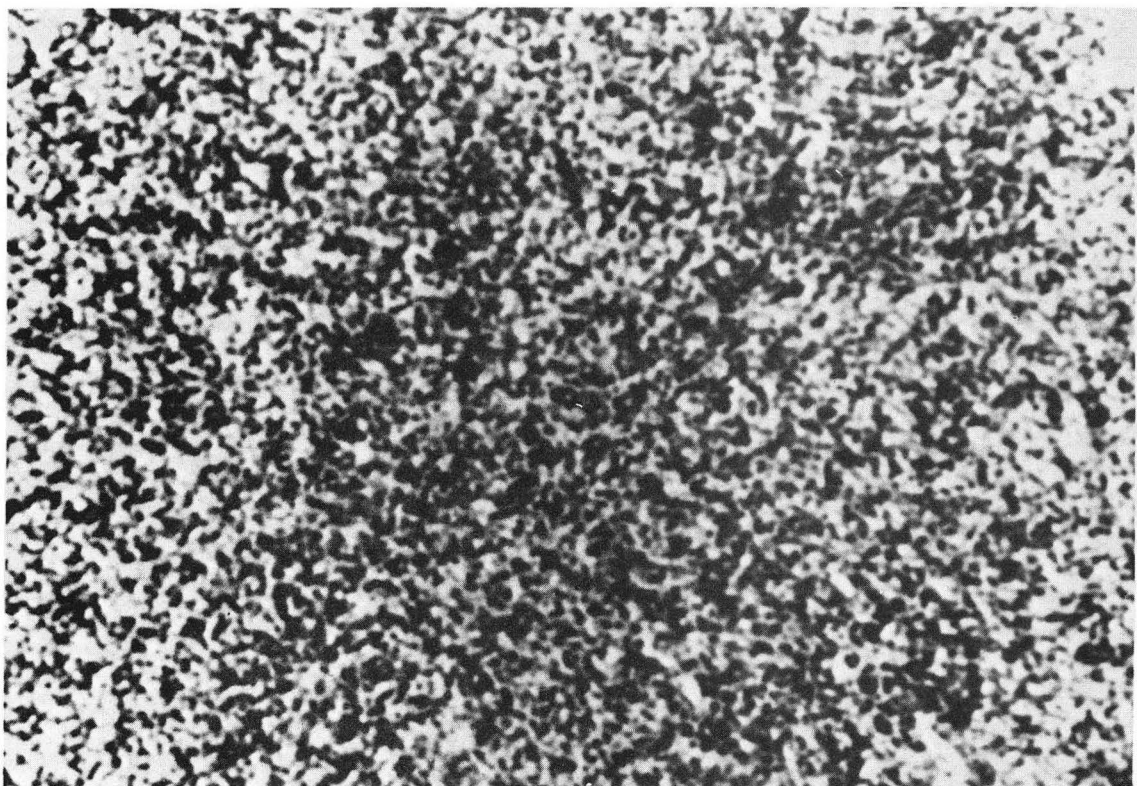
10 μm
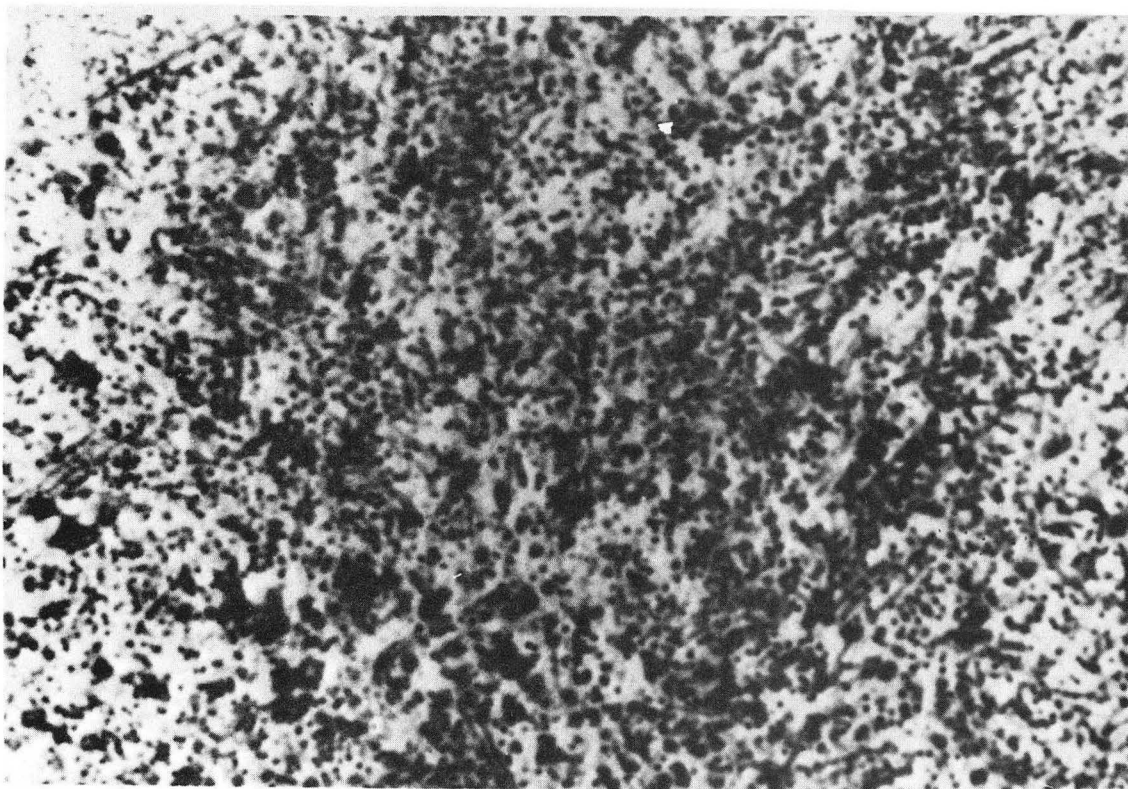
b
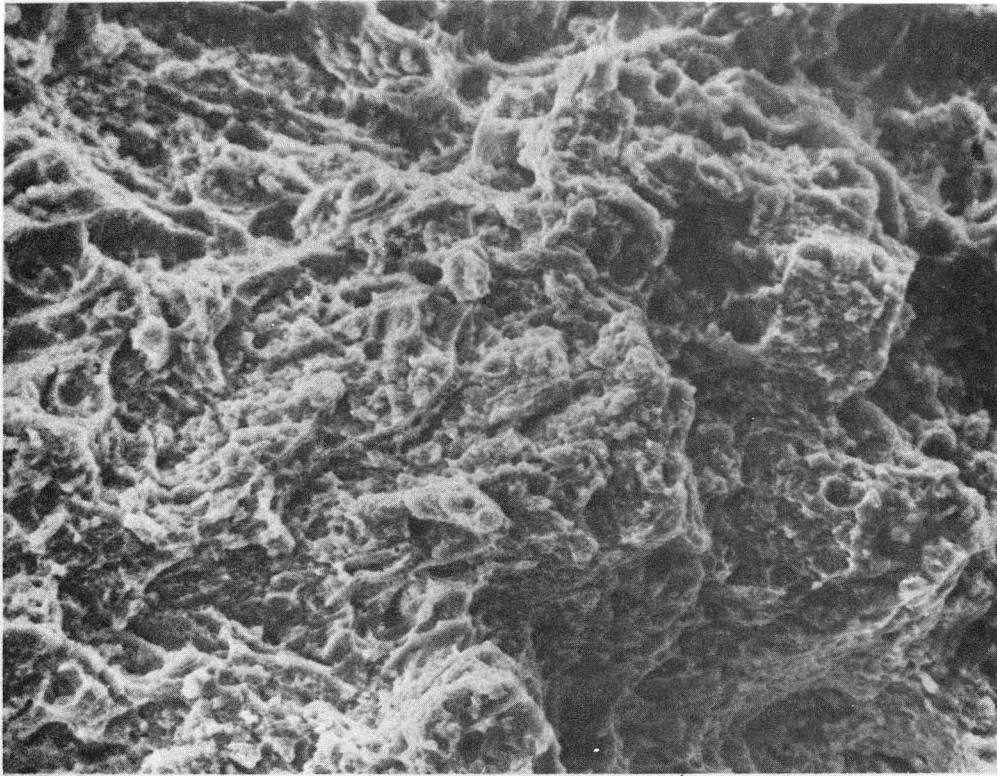
XBB 769-8586

Fig. 10

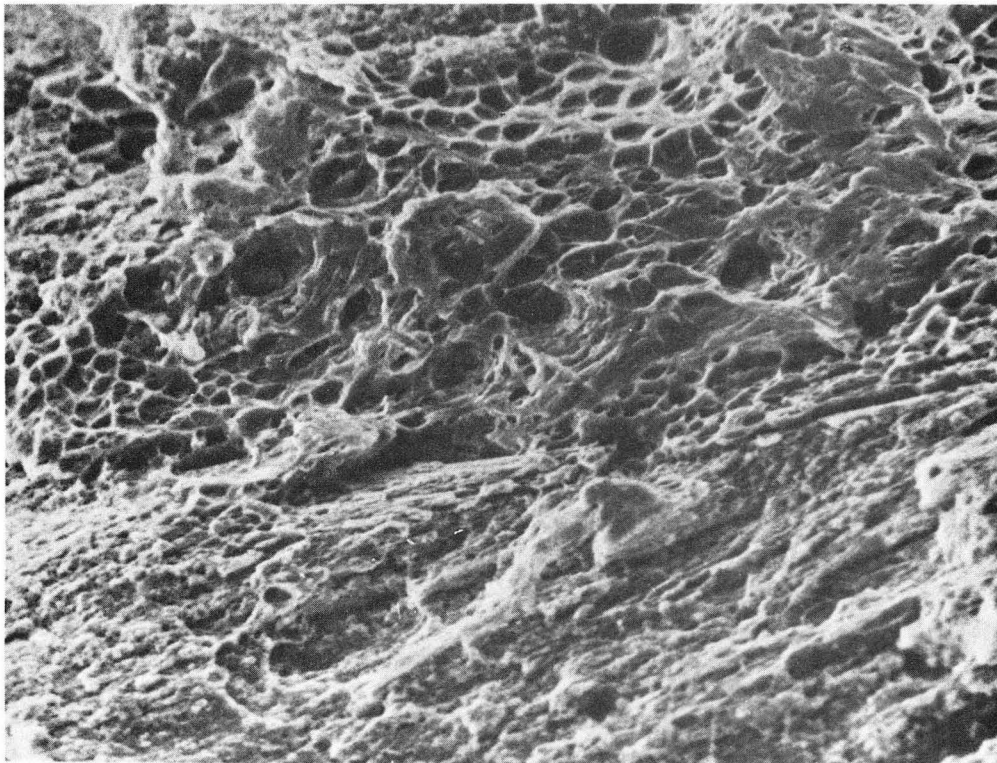a   1 μm

XBB 778-7378

a
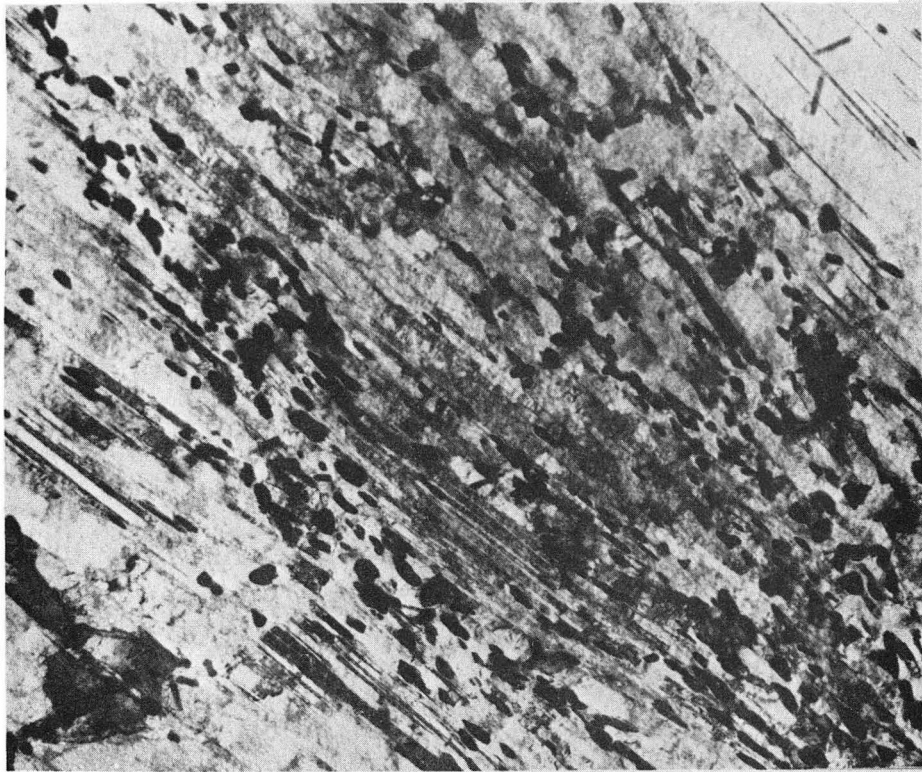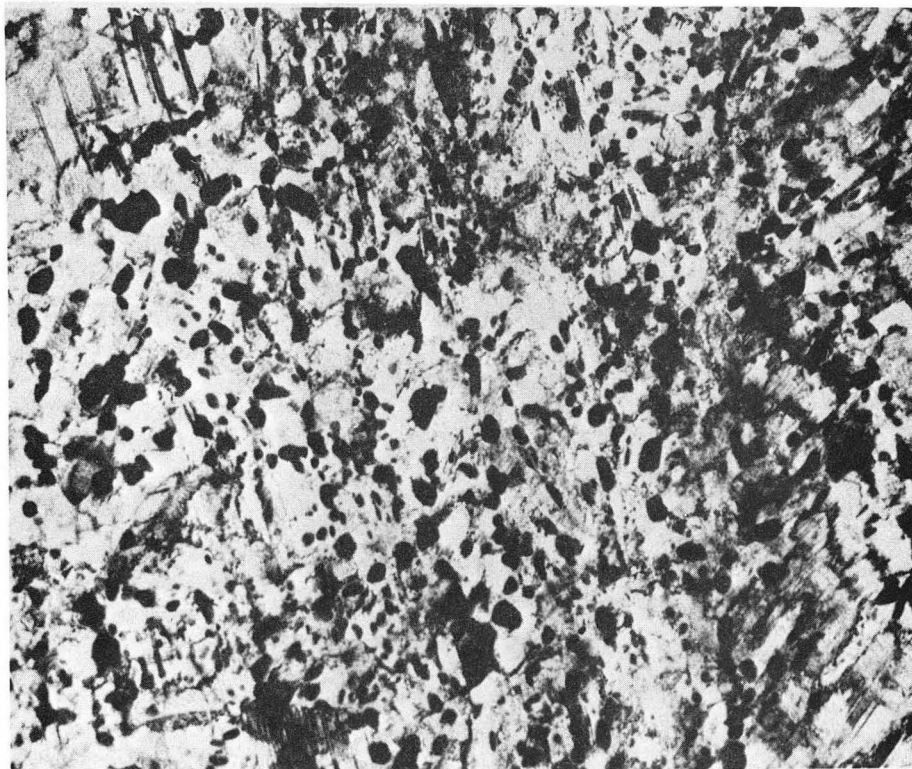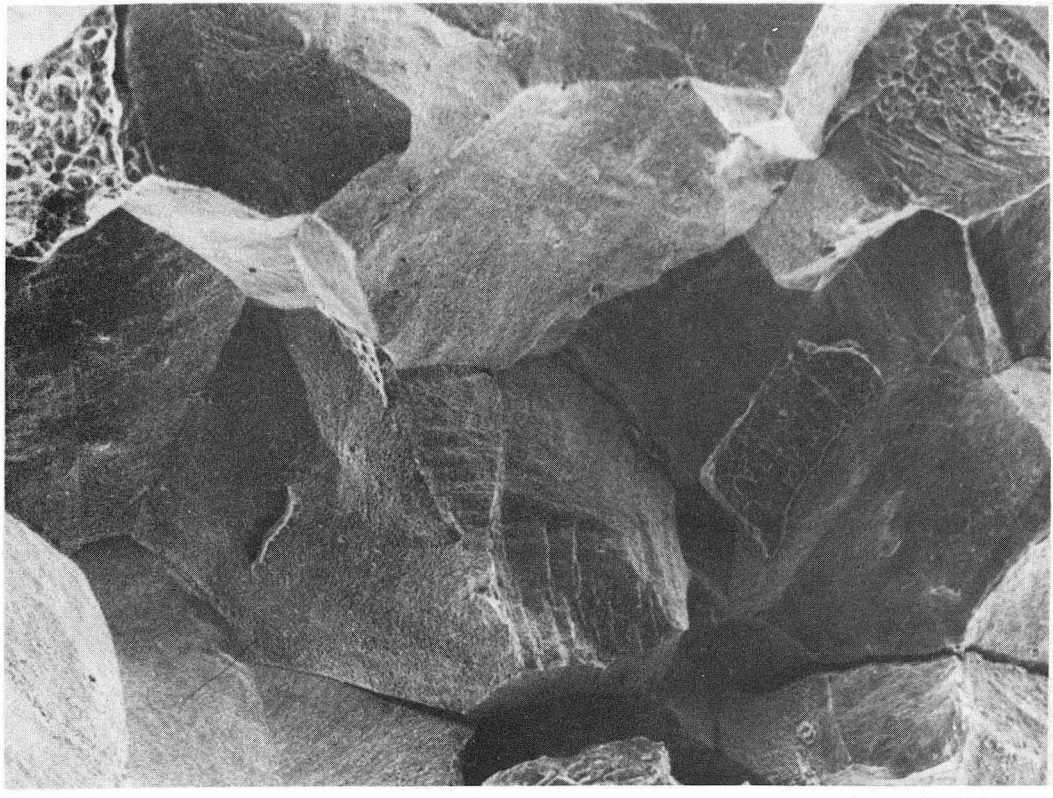
10 μm

b

XBB 760-10566

Fig. 12

XBL778-5877

Fig. 13

XBL778-5876

Fig. 14

a

$10\,\mu m$

b

XBB 788-7377

Fig. 15